Tipping Water Balance in Polymer Electrolyte Fuel Cells with Ultra-Low Pt Loading

Tasleem Muzaffar [1], Thomas Kadyk [2], and Michael Eikerling [1*]

[1] Department of Chemistry, Simon Fraser University, Burnaby, British Columbia, Canada

[2] Institute of Energy and Process Systems Engineering, Technische Universität Braunschweig, Braunschweig, Germany

*meikerl@sfu.ca

Supplementary Information

Table of Contents

Figure S-1, Effect of m_{pt} on σel, $D_{\mathrm{O_2}}^{\mathrm{GDL}}$, $D_{\mathrm{O_2}}^{\mathrm{CCL}}$, and j^0 for all experimental studies .... 2 - 5

Figure S-2, Effect of m_{pt} on σel, $D_{\mathrm{O_2}}^{\mathrm{GDL}}$, $D_{\mathrm{O_2}}^{\mathrm{CCL}}$, and j^0 of data set 2 from Ref 10 and 12 6

Figure S-3, Pol. curve and effect of $\mathrm{m_{pt}}$ on σ_{el}, $\mathrm{D_{O_2}^{GDL}}$, $\mathrm{D_{O_2}^{CCL}}$, and $\mathrm{j^0}$ of study from Breitwieser *et al.* 7

Table S-1, Data of all experimental studies 8

Table S-2, Data of reported diluted studies (both dilution by carbon and mixing two catalyst) 9

Table S-3, List of abbreviations used 10

This section contains the detailed results from the analysis of all experimental data sets evaluated in this study. Physical models developed by Kulikovsky [1, 2] and Sadeghi *et al.* [3] were employed. The analyses revealed a concerted impact of reduced CCL thickness and structural changes incurred by the m_{pt} reduction on a core set of properties including σ_{el}, $D_{\mathrm{O_2}}^{\mathrm{GDL}}$, $D_{\mathrm{O_2}}^{\mathrm{CCL}}$, and j^0. [5-15] Details of GDL type, CCL thickness, and CCL composition in experimental studies are reported in Tables S-1 to S-2.

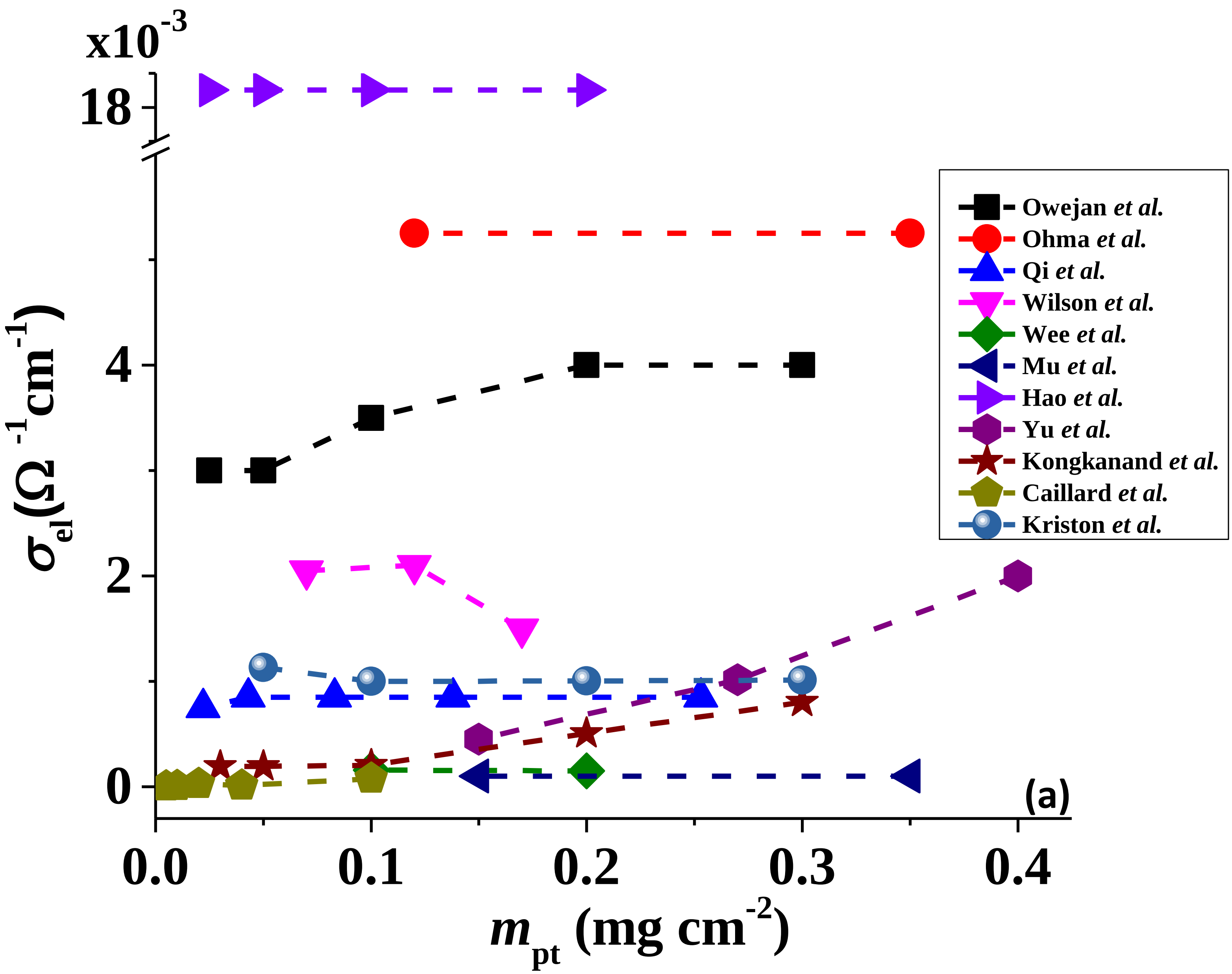

Figure S-1. (a) Effect of m_{pt} on the σ_{el}. σ_{el} remains relatively constant with m_{pt} reduction. Since water is the primary medium for proton conduction, the growth in liquid water saturation upon decreasing m_{pt} does not have a detrimental effect on σ_{el} [5-15]

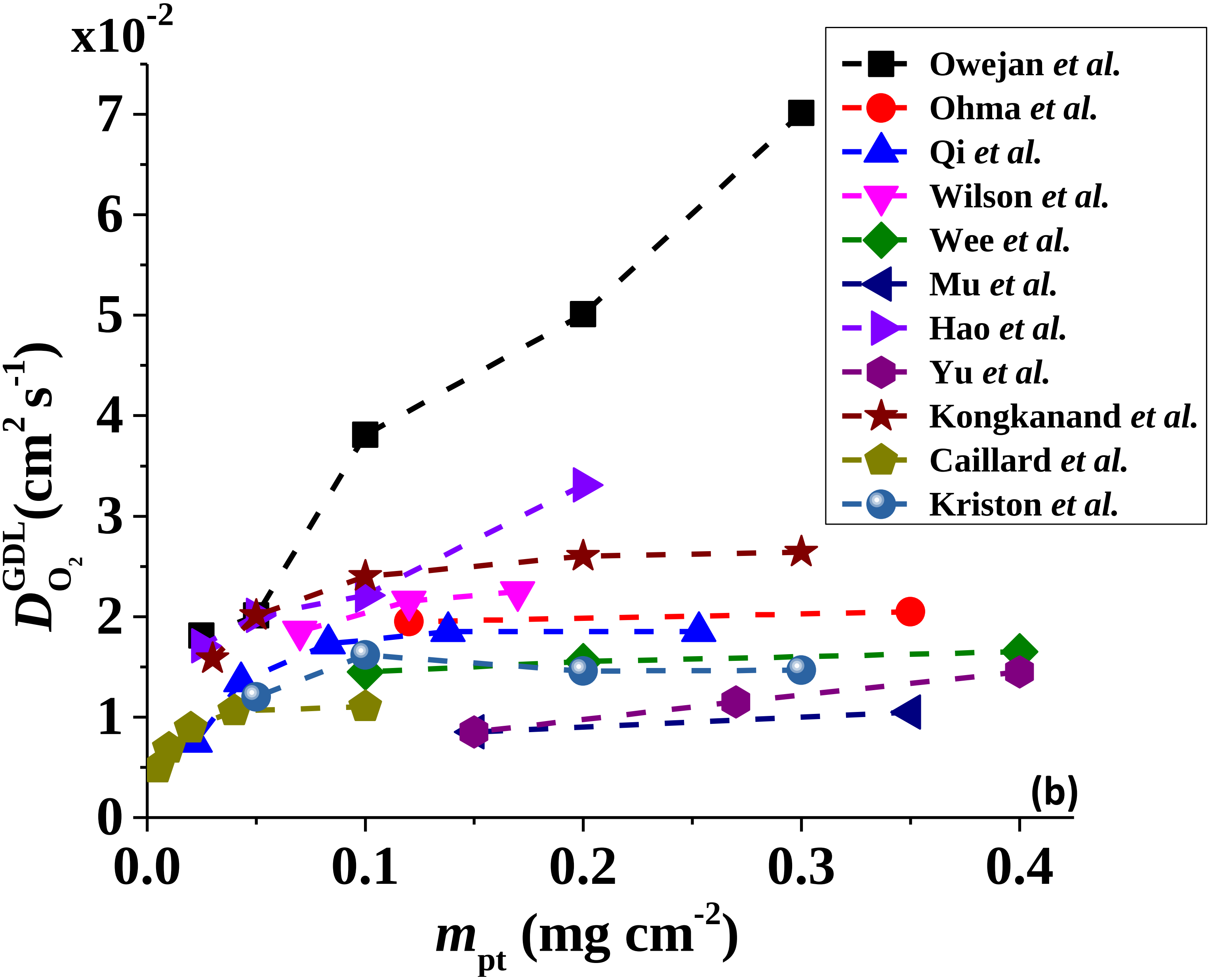

Figure S-1. (b) Effect of m_{pt} on $D_{\mathrm{O_2}}^{\mathrm{GDL}}$. $D_{\mathrm{O_2}}^{\mathrm{GDL}}$ decreases strongly with m_{pt} reduction. Increased liquid water saturation with diminished vaporization capability results in flooding of the GDL which inhibits oxygen diffusion. [5-15]

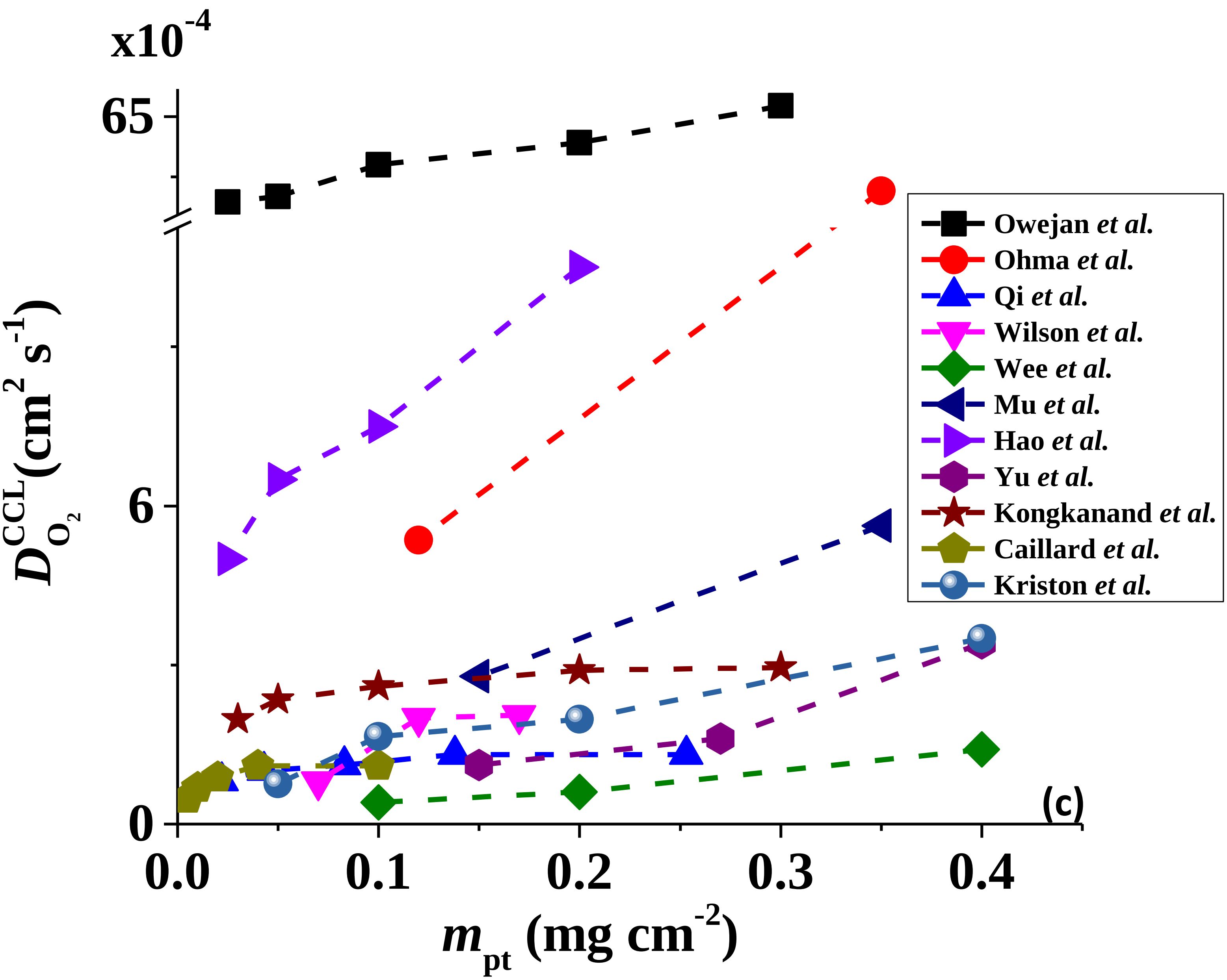

Figure S-1. (c) Effect of m_{pt} on $D_{\mathrm{O_2}}^{\mathrm{CCL}}$. $D_{\mathrm{O_2}}^{\mathrm{CCL}}$ decreases with m_{pt} reduction. Increased liquid water saturation with diminished vaporization capability results in flooding of the CCL which inhibits oxygen diffusion. [5-15]

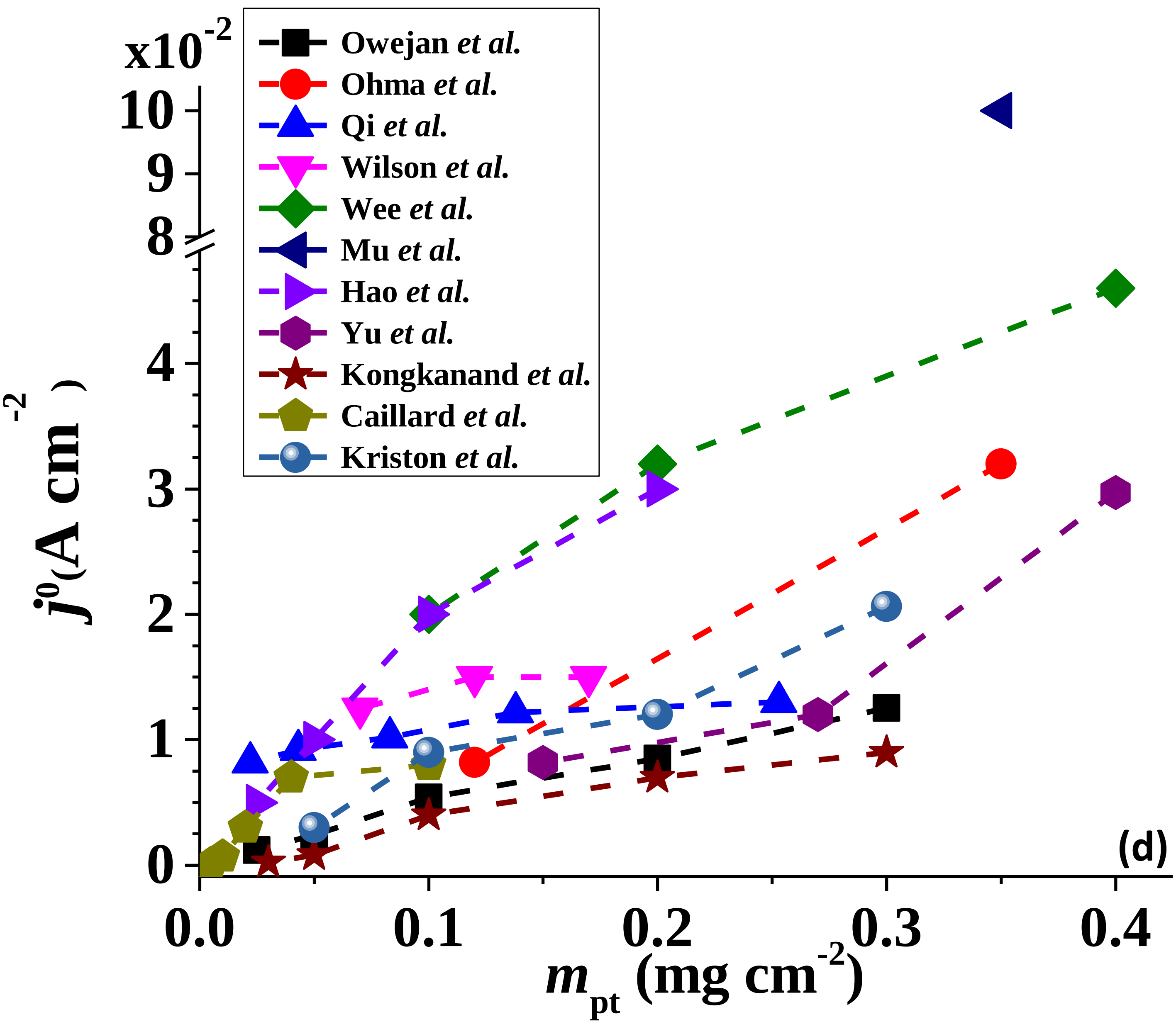

Figure S-1. (d) Effect of m_{pt} on j^0. j^0 follows the trend observed for $D_{\mathrm{O_2}}^{\mathrm{CCL}}$. [5-15]

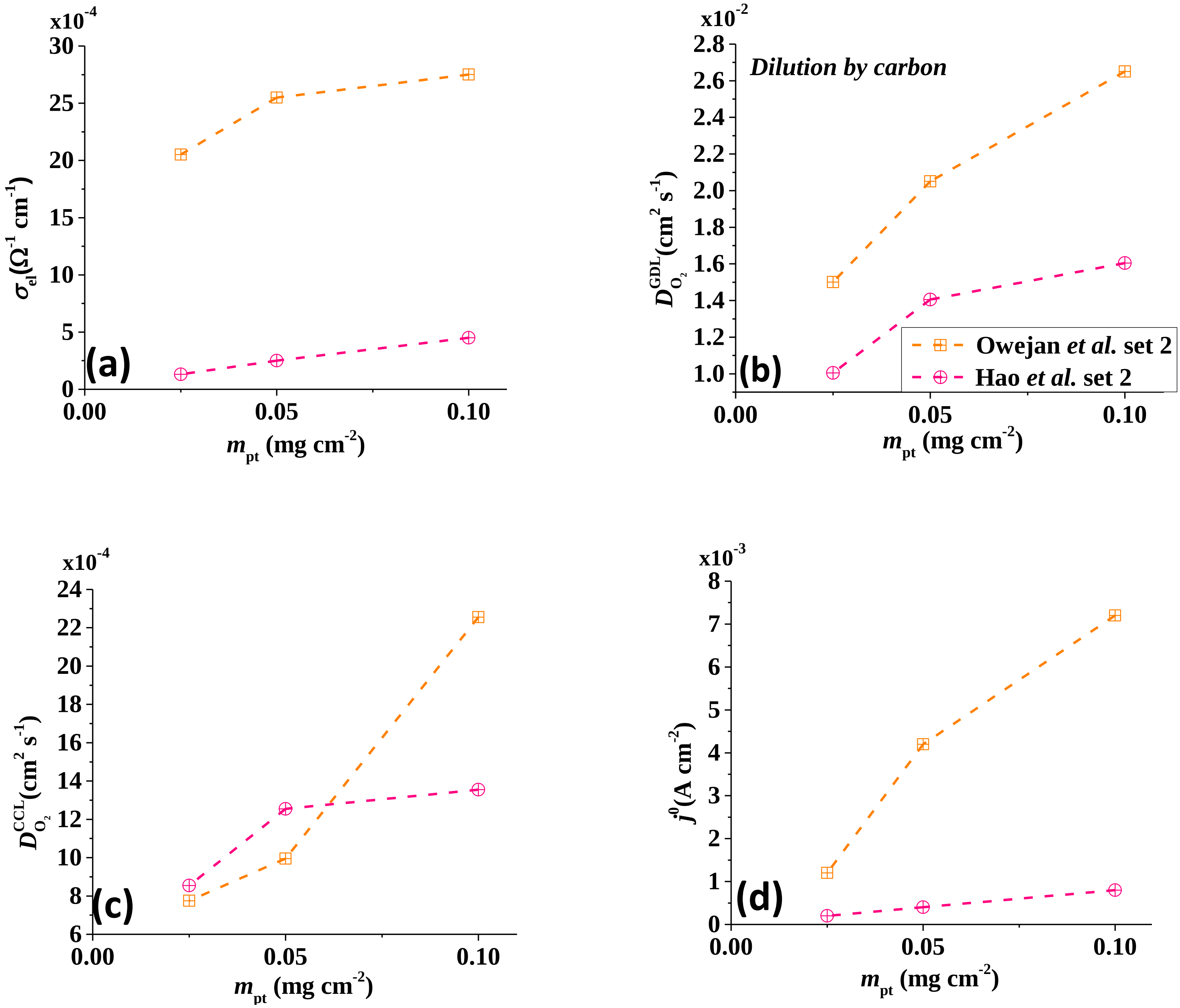

Figure S-2. Effective properties for experimental systems studies for set 2 of Owejan *et al.* [10] and Hao *et al.* [12] i.e. dilution by carbon, including the impact of m_{pt} reduction on (a) σ_{el}, (b) $D_{\mathrm{O_2}}^{\mathrm{GDL}}$, (c) $D_{\mathrm{O_2}}^{\mathrm{CCL}}$, and (d) j^0 .

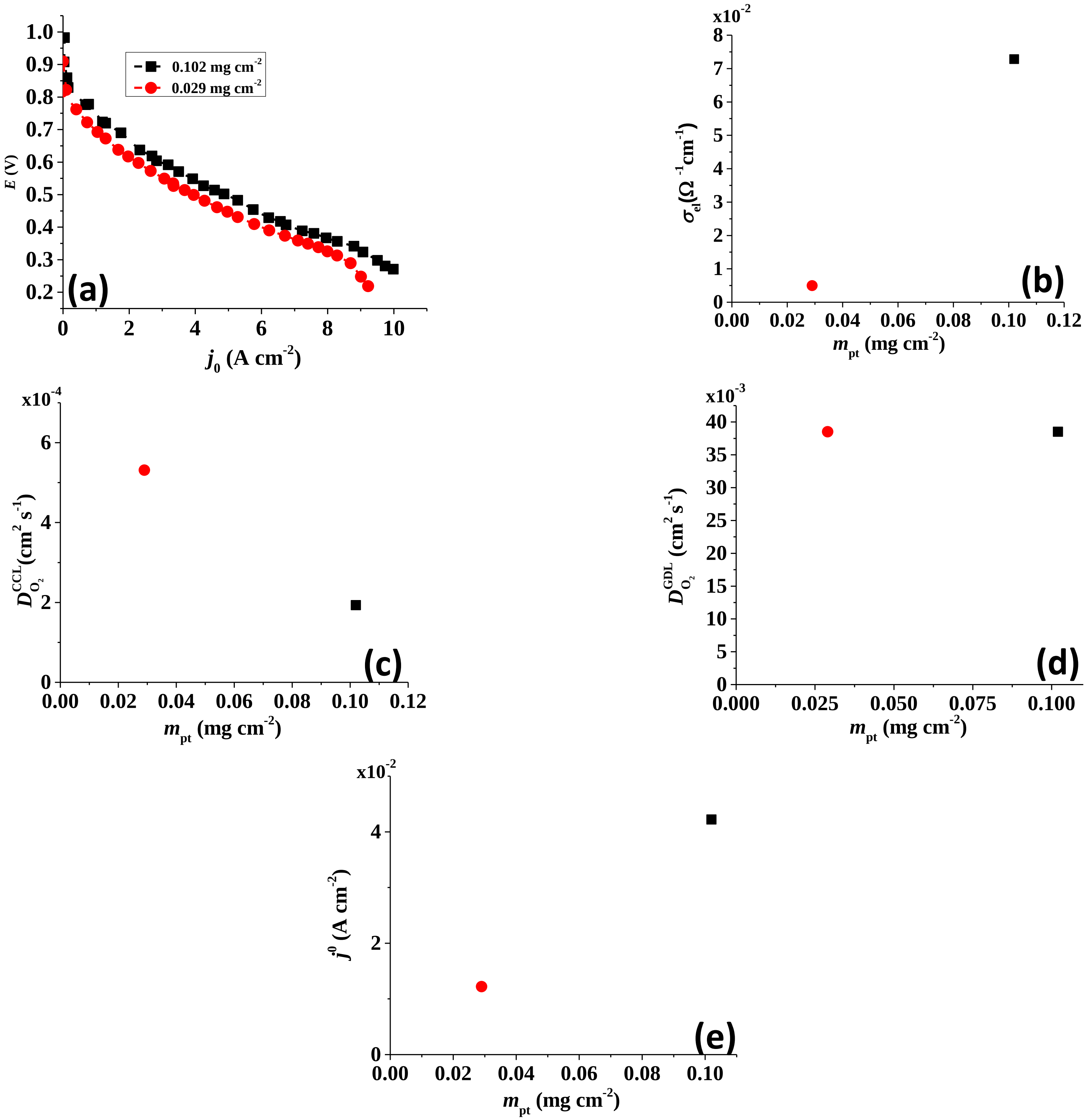

Figure S-3. (a) Polarization curve for MEA fabricated by direct deposition method of Klingele *et al.* [16] and Brietwieser *et al.* [17]. (b-e) shows the effect of m_{pt} reduction on σ_{el}, $D_{O_2}^{GDL}$, $D_{O_2}^{CCL}$, and j^0 respectively. $D_{O_2}^{CCL}, D_{O_2}^{GDL}$ shown in (c) and (d) increases and remains constant with m_{pt} reduction respectively, it is assumed that this effect is caused by the extremely thin and highly permeable PEM employed in the study that enabled highly efficient water removal via the anode. σ_{el} shown in (b) goes down with m_{pt}, this due to highly efficient water removal via the anode. Since water is the primary medium for proton transport.

Table S-1. Data from various study for non-diluted systems

Study	Pt Loading (mgcm^{-2})	Composition (wt%)	Temperature (ºC)	CCL Thickness (µm)	Pt Loading reduction method	Type of GDL	Fabrication Technique	RH %
Kongkanand *et al.* [13]	0.03	50 % Pt/V	80	No Data Available	Non-Diluted	Carbon fiber paper backings	CCM	100
	0.05							
	0.1							
	0.2							
	0.3							
Ohma *et al.* [4]	0.12	30% Pt/C 90% Ionomer /C	80	3.8	Non-Diluted	TGP-H060 (Toray)	Decal Transfer	90
	0.35			11				
Qi *et al.* [6]	0.022	20% Pt/C	45	No Data Available	Non-Diluted	ELAT	Hot Bonding	No Data
	0.043							
	0.083							
	0.138							
	0.253							
Wilson *et al.* [5]	0.07	20% Pt/C	80	2	Non-Diluted	No Data Available	Painting	No Data
	0.12			4				
	0.17			6				
Mu *et al.* [7]	0.15	60% Pt/C	60	~7	Non-Diluted	WUT Energy	CCM	100
	0.35			~7				
Caillard *et al.* [14-15]	0.005	No Data Available	80	2	Non-Diluted	LT1600	Sputtering	Dry
	0.01							
	0.02							
	0.04							
	0.1							
Kriston *et al.* [11]	0.05	46% Pt/C	80	0.942	Non-Diluted	SGL 10 BC	Spray	40
	0.2			No Data Available				
	0.3							

Table S-2. Data from various study for diluted systems

Study	Pt Loading (mgcm^{-2})	Composition (wt%)	Temperature (°C)	CCL Thickness (μm)	Pt Loading reduction method	Type of GDL	Fabrication Technique	RH %
Hao *et al.* [10] set 2	0.025	50% Pt/V; 0.11 – 0.89 C	80	11	Dilution by carbon	No Data Available	Decal Transfer	100
	0.05	50% Pt/V; 0.22 – 0.78 C						
	0.1	50% Pt/V; 0.42 – 0.58 C						
Owejan *et al.* [12] set 2	0.025	50% Pt/V; 0.51 – 0.49 C	80	12.2	Dilution by carbon	Mitsubishi Rayon Co. U-105 (5 wt% PTFE) with MPL	Decal Transfer	100
	0.05	50% Pt/V; 0.22 – 0.78 C		13.1				
	0.1	50% Pt/V; 0.42 – 0.58 C		10.9				
Owejan *et al.* [12]	0.025	5%Pt/V; 1.0	80	11.0±1.2	Dilution by mixing of two catalysts	Mitsubishi Rayon Co. U-105 (5 wt% PTFE) with MPL	Decal Transfer	100
	0.05	10%Pt/V; 1.0		11.2±1.1				
	0.1	30% Pt/V;0.71 – 30% Pt/V; 0.29		10.4±1.8				
	0.2	50% Pt/V; 0.56 – 20% Pt/V; 0.44		9.2±0.8				
	0.3	50 %Pt/V; 0.8 – 10% Pt/V; 0.2		9.7 ±0.2				
Hao *et al.* [10]	0.025	5%Pt/V; 1.0	80	11	Dilution by mixing of two catalysts	No Data Available	Decal Transfer	100
	0.05	10%Pt/V; 1.0						
	0.1	30% Pt/V;0.71 – 30% Pt/V; 0.29						
	0.2	50% Pt/V; 0.56 – 20% Pt/V; 0.44						

Table S-3 List of abbreviations used

PEMFC	Polymer Electrolyte Fuel Cell	MD	Molecular Dynamics
MEA	Membrane Electrode Assembly	NDA	No Data Available
GDE	Gas Diffusion Electrode	Dil	Diluted
FPE	Flooded Porous Electrode	Non-Dil	Non-Diluted
GDL	Gas Diffusion Layer	ECSA	Electrochemical Surface Area
DM	Diffusion Media	S-data	Please Refer to Supporting Information
CCL	Cathode Catalyst Layer	R_{i}	Resistance Through Ionomer Film
GM	General Motors	R_{M}	Resistance Through Flooded Secondary Pores
ORR	Oxygen Reduction Reaction	R_{int}	Resistance of interfacial water layer surrounding the Pt nanoparticle
Pt	Platinum	R_{μ}	Resistance Through Water Filled Primary Pores

References:

[1] Kulikovsky, A. A Physically-Based Analytical Polarization Curve of a PEM Fuel Cell. *J. Electrochem. Soc.* **161**, F263–F270 (2013).

[2] Kulikovsky, A. Analytical Solutions for Polarization Curve and Impedance of the Cathode Catalyst Layer with Fast Oxygen Transport in a PEM Fuel Cell. *J. Electrochem. Soc.* **161**, E3171–E3179 (2014).

[3] Sadeghi, E., Putz, A. & Eikerling, M. Hierarchical Model of Reaction Rate Distributions and Effectiveness Factors in Catalyst Layers of Polymer Electrolyte Fuel Cells. *J. Electrochem. Soc.* **160**, F1159–F1169 (2013).

[4] Ohma, A. et al. Analysis of proton exchange membrane fuel cell catalyst layers for reduction of platinum loading at Nissan. *Electrochim. Acta* **56**, 10832–10841 (2011).

[5] Wilson, M. High Performance Catalyzed Membranes of Ultra-low Pt Loadings for Polymer Electrolyte Fuel Cells. *J. Electrochem. Soc.* **139**, L28–L30 (1992).

[6] Qi, Z. & Kaufman, A. Low Pt loading high performance cathodes for PEM fuel cells. *J. Power Sources* **113**, 37–43 (2003).

[7] Mu, S. & Tian, M. Optimization of perfluorosulfonic acid ionomer loadings in catalyst layers of proton exchange membrane fuel cells. *Electrochim. Acta* **60**, 437–442 (2012).

[8] Wee, J.-H., Lee, K.-Y. & Kim, S. Fabrication methods for low-Pt-loading electrocatalysts in proton exchange membrane fuel cell systems. *J. Power Sources* **165**, 667–677 (2007).

[9] Yu, H., Roller, J., Mustain, W. & Maric, R. Influence of the ionomer/carbon ratio for low-Pt loading catalyst layer prepared by reactive spray deposition technology. *J. Power Sources* **283**, 84–94 (2015).

[10] Hao, L., Moriyama, K., Gu, W. & Wang, C.-Y. Modeling and Experimental Validation of Pt Loading and Electrode Composition Effects in PEM Fuel Cells. *J. Electrochem. Soc.* **162**, F854–F867 (2015).

[11] Kriston, A., Xie, T. & Popov, B. Impact of ultra-low platinum loading on mass activity and mass transport in H_2-oxygen and H_2-air PEM fuel cells. *Electrochim. Acta* **121**, 116–127 (2014).

[12] Owejan, J., Owejan, J. & Gu, W. Impact of Platinum Loading and Catalyst Layer Structure on PEMFC Performance. *J. Electrochem. Soc.* **160**, F824–F833 (2013).

[13] Kongkanand, A., Subramanian, N., Yu, Z., Y.and Liu, Igarashi, H. & Muller, D. Achieving High-Power PEM Fuel Cell Performance with an Ultralow-Pt-Content Core-Shell Catalyst. *ACS Catal*. **6**, 1578–1583 (2016).

[14] Caillard, A., Charles, C., Boswell, R. & Brault, P. Improvement of the sputtered platinum utilization in proton exchange membrane fuel cells using plasma-based carbon nanofibres. *J. Phys. D. Appl. Phys.* **41**, 185307–185316 (2008).

[15] Caillard, A., Charles, C., Ramdutt, D., Boswell, R. & Brault, P. Effect of Nafion and platinum content in a catalyst layer processed in a radio frequency helicon plasma system. *J. Phys. D. Appl. Phys.* **42**, 045207–045215 (2009).

[16] Klingele, M., Breitwieser, M., Zengerle, R. & Thiele, S. Direct deposition of proton exchange membranes enabling high performance hydrogen fuel cells. *J. Mater. Chem. A.* **3**, 11239–11245 (2015).

[17] Breitwieser, M., Klingele, M., Vierrath, S. & Klose, C. Direct membrane deposition for high performance hydrogen fuel cells. *IMTEK Present*. CaRPE (2014).